American Mineralogist, Volume 101, pages 2367–2376, 2016

INVESTIGATING PETROLOGIC INDICATORS OF MAGMATIC PROCESSES IN VOLCANIC ROCKS

Nucleation rates of spherulites in natural rhyolitic lava

James E. Gardner[1,*], Kenneth S. Befus[2], James M. Watkins[3], and Travis Clow[1]

[1]Department of Geological Sciences, Jackson School of Geosciences, The University of Texas at Austin, Austin, Texas 78712-0254, U.S.A.
[2]Department of Geosciences, Baylor University, Waco, Texas 76798, U.S.A.
[3]Department of Geological Sciences, University of Oregon, Eugene, Oregon 97403-1272, U.S.A.

Abstract

The rates of nucleation and crystal growth from silicate melt are difficult to measure because the temperature–time path of magma is often unknown. We use geochemical gradients around spherulites in obsidian glass to estimate the temperature–time interval of spherulite crystallization. This information is used in conjunction with new high-resolution X-ray computed tomography (HRXCT) data on the size distributions of spherulites in six samples of rhyolite obsidian lava to infer spherulite nucleation rates. A large data set of geochemical profiles indicate that the lavas cooled at rates of $10^{-2.2}$ to $10^{-1.2}$ °C/h, and that the spherulites grew at rates that decreased exponentially with time, with values of $10^{-0.70}$ to $10^{0.30}$ μm/h at 600 °C. Spherulites are estimated to have begun nucleating when undercooling [ΔT, = liquidus T (≈800 °C) minus nucleation T] reached 100–277 °C, and stopped when ΔT = 203–365 °C, with exact values dependent on assumed cooling and growth rates. Regardless of rates, we find that spherulites nucleated within a ~88–113 °C temperature interval and, hence, began when $\Delta T \approx 0.65–0.88 \times T_L$, peaking when $\Delta T \approx 0.59–0.80 \times T_L$. A peak rate of nucleation of 0.072 ± 0.049 cm^{-3} h^{-1} occurred at 533 ± 14 °C, using cooling and growth rates that best fit the data set of geochemical profiles. While our inferred values for ΔT overlap those from experimental studies, our nucleation rates are much lower. That difference likely results from experimental studies using hydrous melts; the natural spherulites grew in nearly anhydrous glass.

Keywords: Spherulite, nucleation rate, growth rate, cooling rate, Yellowstone, obsidian, Invited Centennial article

Introduction

Crystallization of molten magma affects magma rheology and volatile exsolution, and it has been long thought to be a dominant process in generating the vast array of magma compositions seen on Earth (e.g., Bowen 1919, 1947; McKenzie 1984). Despite the importance of crystallization to many problems in igneous petrology and volcanology, the kinetics of crystallization, and hence the rate at which magma undergoes physical and chemical changes, are not well understood. Much of our knowledge on crystallization comes from laboratory experiments, where temperature and cooling rate are controlled. There are, however, limits to laboratory investigations. For one, it is not yet possible to observe the onset of crystallization because nucleation clusters consist of only tens to thousands of atoms (Lasaga 1998). It is also difficult to measure the kinetics of crystallization in highly viscous melts because of the long run times needed to achieve visible crystals (e.g., Schairer and Bowen 1956; Johannes 1979). Experiments on crystal nucleation in viscous melts are also few because of their significant incubation periods, where melts can be held for significant times below their liquidi and not produce recognizable crystals (Winkler 1947; Schairer and Bowen 1956; Fenn 1977; Lofgren 1974; Swanson 1977). The incubation period is the time it takes a system to re-establish an equilibrium cluster-size distribution in response to a sudden change in temperature or pressure (Turnbull 1948). During that adjustment period, the likelihood that a cluster of critical size can be formed is extremely low. Incubation periods thus introduce large uncertainties in determining the onset of nucleation (e.g., Swanson 1977; Fenn 1977).

One way of overcoming some of the experimental limitations is to deduce crystallization rates from natural samples. Natural lavas, for example, can crystallize over much longer periods of time than experimental samples. Crystal-size distributions (CSD) of natural samples have thus been used to infer crystallization rates (e.g., Marsh 1988, 1998, 2007; Cashman and Marsh 1988; Higgins 1999; Morgan et al. 2007). A CSD is described using a population density function $n = dN/dL$, where N is the cumulative number of crystals per unit volume and L is the linear crystal size. The slope and intercept on a plot of $\ln(n)$ vs. L contains information on the average nucleation rate and average growth rate (e.g., Cashman and Marsh 1988). Use of such methods, however, provides only time-averaged crystallization rates, and requires that the temperature–time interval of crystallization can be constrained independently.

* E-mail: gardner@mail.utexas.edu
Special collection information can be found at http://www.minsocam.org/MSA/AmMin/special-collections.html.

In this study we use a different approach to derive nucleation rates for spherulites in rhyolite lavas. Spherulites—radiating aggregates of crystals—were analyzed in three dimensions using X-ray computed tomography, providing the full size of each spherulite and their volumetric number density. To interpret the size distributions in terms of nucleation kinetics, we derive the time frame for nucleation and the thermal conditions for crystallization from modeling geochemical gradients around the spherulites (Gardner et al. 2012; Befus et al. 2015b). We target spherulites in Yellowstone rhyolite obsidian lavas, because they are all dense aggregates of radiating sanidine and quartz (plus minor amounts of Fe-Ti oxides) that grew in high-silica rhyolite melt under similar thermal histories. Many variables that impact crystallization kinetics are thus similar between samples.

Methods

Six fist-sized samples were collected from three different lava flows (Pitchstone Plateau, Summit Lake, and Solfatara Plateau) for this study (Fig. 1). One sample was collected from near the mapped vent region of each flow (Y-22, Y-80, Y-200; Table 1), while the other three come from either the flow front (Y-202 from Summit Lake and Y-142 from Solfatara Plateau) or a significant distance away from vent (Y-193 from Pitchstone Plateau). These lavas erupted between ~70 and 120 ka (Christiansen 2001; Christiansen et al. 2007). A rectangular block ~3 cm per side was sawed from each sample, and scanned at the University of Texas High-Resolution X-ray Computed Tomography (HRXCT) facility. The data were acquired using a Zeiss (formally Xradia) microXCT 400 operating at 60 kV and 8 W with a 0.35 mm SiO_2 X-ray prefilter. All scans were reconstructed as 16-bit TIFF stacks with a resulting voxel (3D pixel) resolution of 25.07 µm. Spherulites in the resulting grayscale images do not contrast greatly from the surrounding matrix as a result of similar attenuation values, which made automated segmentation and analysis not viable. Instead, each scan was imported into Avizo 8.0 for manual segmentation, utilizing various software tools built into the program (Fig. 2). Each spherulite was visually identified and segmented into three orthogonal slices; more slices were used for relatively large spherulites and those not roughly spherical to better capture their actual shapes. The slices were used to measure the full 3D dimensions of each spherulite. When spherulites were touching, segmentation was used to manually separate them before analysis. Once segmented, each was saved individually and imported into the Blob3D software (Ketcham 2005) for data extraction (Fig. 2). Best-fit ellipsoids were fitted to the previously segmented slices to measure the volume of each spherulite. Uncertainty on volume measurements is controlled by the voxel size relative to the spherulite diameter, but is thought to be on order of

Table 1. Spherulite sizes and amounts

Sample	Average[a] (mm³)	Median[a] (mm³)	Largest[a] (mm³)	Smallest[a] (mm³)	N_S[b] (cm⁻³)	n[c]	φ[d] (vol%)
Y22	0.9726	0.3551	28.74	0.0074	256.2	652	13.70
Y80	0.4624	0.1910	17.59	0.0057	314.4	1190	14.53
Y142	0.9757	0.3073	49.60	0.0120	125.5	809	12.24
Y193	2.1535	0.4371	58.37	0.0140	74.4	480	16.02
Y200	3.3506	0.6644	120.4	0.0100	88.0	489	29.47
Y202	3.2969	0.9961	459.9	0.0130	110.1	525	36.28

[a] Average, median, largest, and smallest volumes of spherulites, in cubic millimeters.
[b] N_S = number density of spherulites, in number per cubic centimeters.
[c] n = number of spherulites measured.
[d] φ = volume percent of spherulites in the sample.

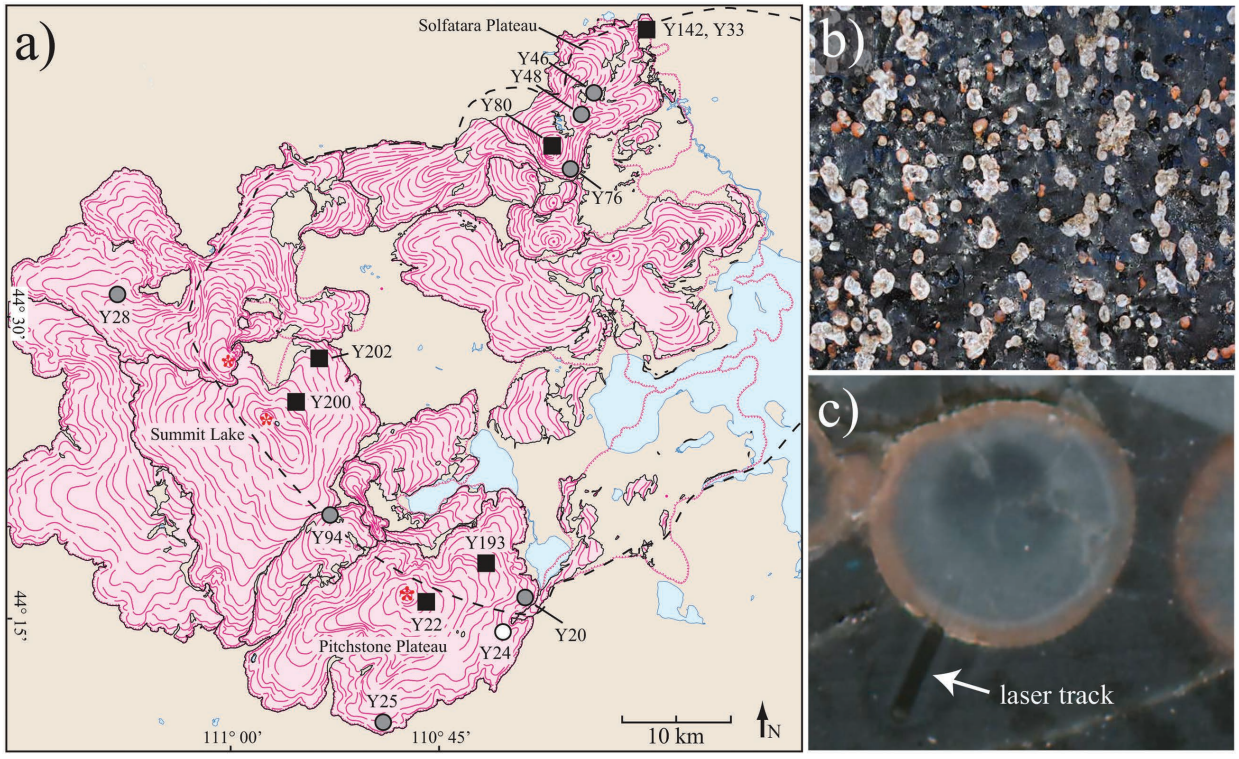

Figure 1. (**a**) Simplified geologic map of Central Plateau Member rhyolites in the Yellowstone caldera, Wyoming, modified after Christiansen (2001). Lava flows are shown in pink, with sampled lavas labeled and positions where samples were collected (black squares for samples scanned by HRXCT; gray circles are additional samples for geochemical data; white circle is Y24 from Befus et al. 2015b, also included in this study). (**b**) Representative photograph of Yellowstone spherulites from Solfatara Plateau lava, photographed near Y142 in **a**. Field of view is approximately 10 cm across. (**c**) Photomicrograph of a representative spherulite (in sample Y202) analyzed for geochemical gradients. For scale, the laser track highlighted is 100 µm wide. The gradation in color in the spherulite probably results from oxidation.

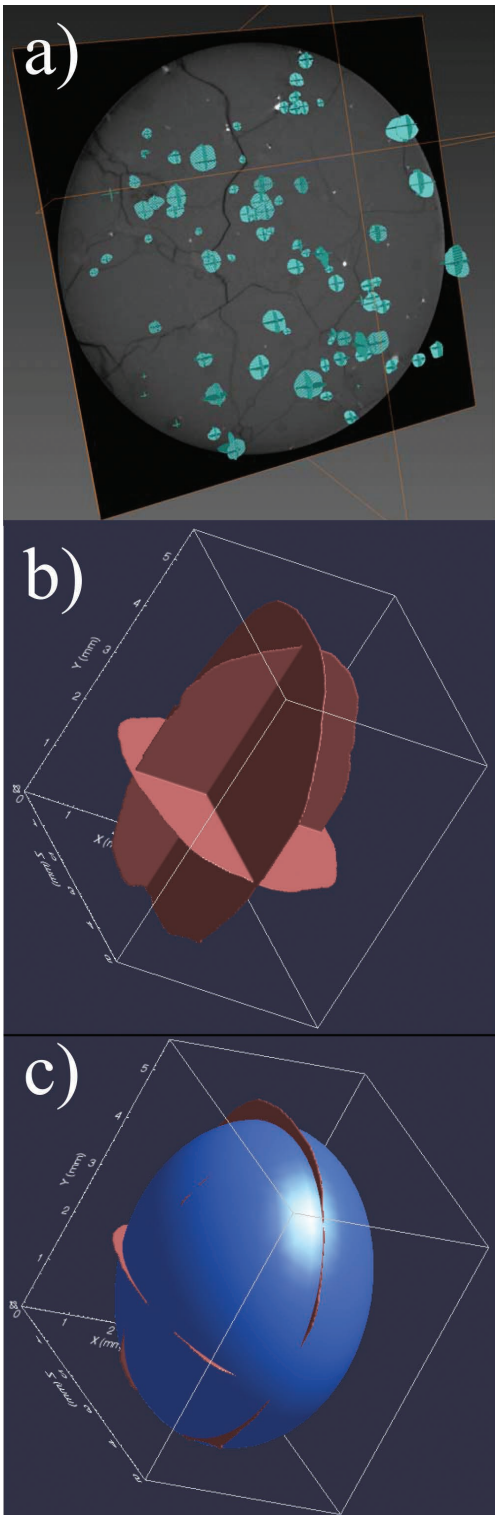

FIGURE 2. Image illustrating steps used to measure spherulite volumes. (**a**) Spherulites manually segmented in Aviso using three orthogonal planes to represent their volumes, shown in relationship to a tomography slice. (**b**) Segmented planes were transported into Blob3D to verify that all spherulites were separated. (**c**) Best-fit ellipsoids for each spherulite were generated using Blob3D. Ellipsoid shown is fit to the orthogonal planes shown in **b**. The volume of each ellipsoid was then measured.

about 1% of the total volume (Hanna et al. 2015). A total of 480–1190 spherulites were measured in each sample (Table 1). For convenience, we report the equivalent spherical diameter for each spherulite calculated from its volume.

Thick sections were cut from each sample block and polished for geochemical analysis. One to three spherulites were targeted in each sample, chosen to cover a broad range of sizes. Each section was oriented so that the centers of the targeted spherulites were exposed. This was achieved by first knowing where targeted spherulites were in the blocks, based on the CT scans, and then slowly grinding the section until the size of the targeted spherulites stopped increasing, indicating that the center had been reached. The geochemical analyses, which were measured along traverses perpendicular to the edge of the spherulites, were thus perpendicular to the full diameter of the spherulite. The widths of individual crystals inside spherulites were measured using a petrographic microscope.

To augment our data set an additional 54 analyses of spherulite-matrix glass pairs are included from 14 other samples from Yellowstone lavas (Befus et al. 2015b; Befus, unpublished data). We followed the same analytical methods as reported in Gardner et al. (2012) and Befus et al. (2015b). Briefly, trace-element concentrations were measured using LA-ICP-MS at the University of Texas at Austin, using a New Wave Research UP 193-FX fast excimer (193 nm wavelength, 4–6 ns pulse width) laser system coupled to an Agilent 7500ce ICP-MS. Reference standards and rhyolite sections were sampled as line scans (5 µm/s), using a rectangular 5 × 50 µm slit aperture oriented with long-axis normal to the scan direction, which was oriented normal to the local margin of the spherulite and glass (Fig. 1). The ICP-MS monitored masses ^{7}Li, ^{11}B, ^{23}Na, ^{25}Mg, ^{29}Si, ^{39}K, ^{45}Sc, ^{55}Mn, ^{59}Co, ^{85}Rb, ^{88}Sr, ^{133}Cs, ^{137}Ba, and ^{208}Pb at a reading every 3.73 µm. Time-resolved intensities were converted to concentration (parts per million) equivalents using Iolite software (University of Melbourne), with ^{29}Si as the internal standard, and a Si index value of 35.8 wt%. Based on recoveries among analytes we conservatively assign 5% as relative uncertainties.

SPHERULITES AND THEIR ASSOCIATED GEOCHEMICAL GRADIENTS IN YELLOWSTONE RHYOLITIC LAVAS

Spherulites in all samples consist of radiating masses of intergrown sanidine and quartz crystals, with minor amounts of Fe-Ti oxides and glass (Fig. 1). In most cases, sanidine and quartz crystals are elongated roughly perpendicular to the outer margin of the spherulite (Fig. 3). In the cores of the largest spherulites individual crystals are 29 ± 5 µm wide. Near the rims of those same spherulites, however, individual crystals are only 8 ± 2 µm wide. In the smallest spherulites, crystals are smaller, 10 ± 3 and 7 ± 1 µm in spherulite cores and rims, respectively. Note that crystals throughout small spherulites are similar in size to those near the rims of large spherulites (Fig. 3).

The largest spherulites measured have volumes that range from 17.6 to 459.9 mm^3, depending on the sample (Table 1). The smallest spherulites measured have volumes ranging from 0.0057 to 0.013 mm^3. There are smaller spherulites in all samples, but these were smaller than analytical resolution. We note that their numbers are few compared to the measured population of spherulites, as shown by the size distributions (Fig. 4). Overall, the equivalent spherical diameter of spherulites ranges from ~220 to ~9580 µm. The median volume is ~0.191 to ~0.996 mm^3, or ~715 to ~1240 µm in diameter.

Spherulite size distributions are mainly unimodal, with the most common spherulites in all samples being ~660–1020 µm in diameter (Fig. 4). These make up ~50–60% of the populations in the Pitchstone Plateau and Solfatara Plateau samples and ~35–40% of the Summit Lake samples. All populations are positively skewed, with relatively large spherulites making up different proportions of the populations in different samples. For example, spherulites larger than 880 µm make up 24–29% of the populations in the Summit Lake samples, but only 2–17% in the others. In general, Summit Lake samples contain larger

spherulites, and in fact one sample (Y202) has a secondary mode in size at ~1500 µm. Despite such differences, number densities of spherulites from all three flows overlap and range from ~74 to ~314 cm^{-3} (Table 1).

A total of 63 spherulite–matrix glass pairs were analyzed, and all show similar geochemical patterns (Fig. 5). Concentrations of Li are uniformly low within spherulites (7 ± 4 ppm), and uniformly high in the surrounding glass (58 ± 5 ppm). The change is sharp, occurring over a distance of <10 µm, and coincides with the margin of the spherulite. Concentrations of Rb are also relatively low inside spherulites (113 ± 33 ppm), and larger spherulites typically have slightly less Rb in them than smaller ones. Far away from spherulites the glasses in all samples have uniformly high Rb contents of 225 ± 22 ppm (Fig. 5). Unlike Li, Rb contents vary in the matrix, with the maximum concentration occurring at the contact with the spherulite and decreases over a distance of ~190–390 µm to the far-field value (Fig. 5). Both the enrichment of Rb at the margin and the distance over which elevated concentrations are found in the glass correlate with the size of the spherulite. Measured concentrations of Rb for all spherulite–matrix pairs are listed in the Supplemental[1] Data Table. It is thought that Rb inside the spherulites is contained in the feldspars and/or any remaining glass. All other elements have variable but similar abundances inside and outside of the spherulites (Fig. 5). There are spikes in concentrations found at the outer edges of some spherulites, most commonly in Mg, Cs, Ba, Sr, and Pb.

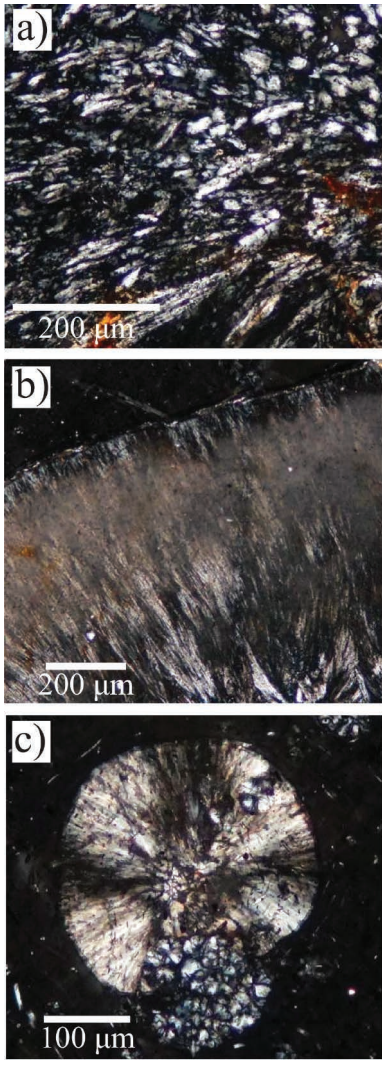

Figure 3. Photomicrographs of crystals in Yellowstone spherulites. (**a** and **b**) Crystals in the core and rim, respectively, of spherulite Y80 T1, which is 2950 µm in diameter. Scale bar is 200 µm long. (**c**) Crystals in spherulite Y80 T2, which is 300 µm in diameter. Scale bar is 100 µm long.

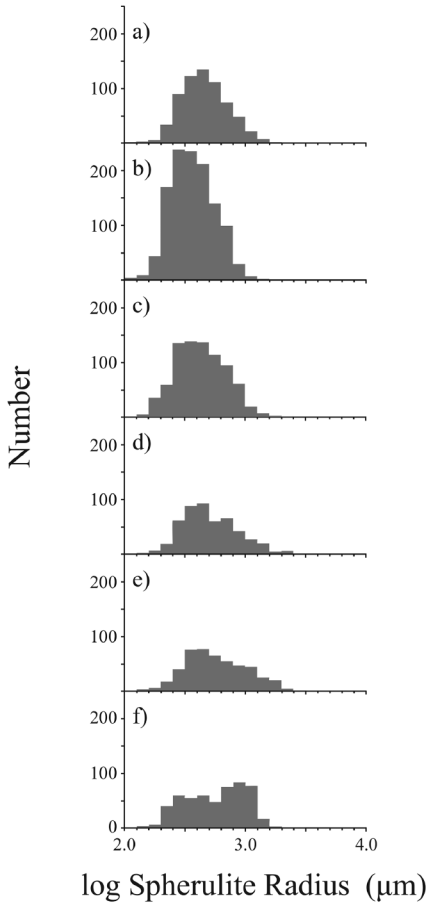

Figure 4. Spherulite size distributions. (**a**) Y22; (**b**) Y80; (**c**) Y142; (**d**) Y193; (**e**) Y200; and (**f**) Y202.

Discussion

The fact that spherulites of all sizes are approximately spherical indicates that they grew after lava had been emplaced and ceased to deform. Because all spherulites in a given sample experience the same thermal history, it is reasonable to assume that (1) all spherulites in a given sample stopped growing at the same time/temperature, and (2) larger spherulites are larger because they nucleated earlier, and thus at higher temperature, and were growing for longer periods of time than smaller spherulites.

[1]Deposit item AM-16-115624, Supplemental Data. Deposit items are free to all readers and found on the MSA web site, via the specific issue's Table of Contents (go to http://www.minsocam.org/msa/ammin/toc/2016/Nov2016_data/Nov2016_data.html).

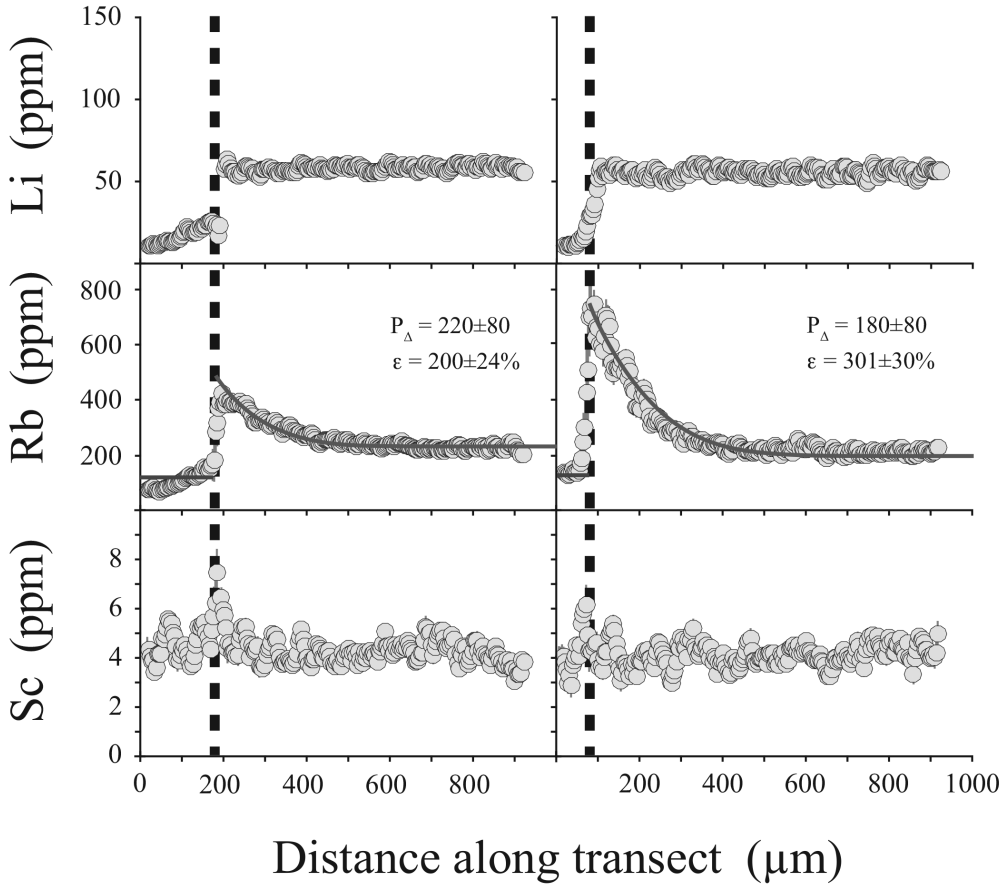

FIGURE 5. Example concentrations of Li, Rb, and Sc in spherulite and matrix glass as a function of distance. The boundary between spherulite and matrix is marked with the dotted lines. The left-hand column shows elemental concentrations associated with Y193 T1 (585 μm diameter); the right-hand column is Y142 T1 (2030 μm diameter). The enrichment (ε) of Rb at the margins and the propagation distance (P_Δ in μm) are listed for each. Predicted variations in Rb concentration from the moving boundary diffusion model are shown as gray curves, calculated using best-fit rates for growth (1.0 ± 0.5 μm/h) and cooling ($10^{-1.6}$ ± 0.3 °C/h).

Thus, with knowledge of spherulite growth rates and thermal histories, one can use spherulite size distributions to reconstruct nucleation rate vs. temperature curves.

Recent studies have shown that compositional gradients associated with spherulites in rhyolitic lavas formed during their growth while the lava cooled (Castro et al. 2008; Watkins et al. 2009; Gardner et al. 2012; Befus et al. 2015b; Befus 2016). The style of gradient for a given element can be understood in terms of its relative compatibility and diffusivity, growth kinetics of the spherulite, and the thermal conditions of the lava (Smith et al. 1955; Albarede and Bottinga 1972; Skora et al. 2006; Watson and Muller 2009; Gardner et al. 2012; Befus et al. 2015b). Briefly, while lava cools elements that diffuse fast relative to the growth rate of the spherulite are expected to have different abundances inside and outside of the spherulite, based on their compatibility with the crystals forming the spherulite, but there will be no gradients in concentration in either; for convenience, we refer to these as Type 1 gradients. On the other hand, elements that diffuse significantly slower than the spherulite grows are expected to have constant abundances across the spherulite and matrix, which we refer to as Type 3 gradients. In between, there are some incompatible elements that can diffuse slightly faster than the spherulite can grow, and hence they become concentrated at the migrating spherulite–matrix boundary. The elevated concentrations lead to diffusion away from the boundary, resulting in decreasing concentrations out into the glass until the far-field concentration is reached; we refer to these gradients as Type 2. Studies of spherulites in rhyolite lavas indicate that concentrations of Rb and H_2O commonly occur in Type 2 gradients (Castro et al. 2008; Watkins et al. 2009; Gardner et al. 2012; Befus et al. 2015b).

Compositional gradients can be modeled using a moving boundary diffusion model that incorporates the growth rate of the spherulite, thermal conditions during its growth, and the diffusion rate of the element (Gardner et al. 2012). Here, we use a model in which radial spherical growth decreases as a function of temperature, following

$$(dR/dt) = (dR/dt)_0 \cdot \exp[-\alpha \cdot (T - T_o)] \quad (1)$$

where (dR/dt) is the radial growth rate at a specific time step, $(dR/dt)_o$ is the initial radial growth rate, T is temperature at time t, and T_o is initial temperature. The parameter a is set to 0.025

to generate an exponential decay in growth rate (Befus et al. 2015). This growth model was shown to best fit the overall differences in elemental enrichment at spherulite–matrix boundaries of spherulites in rhyolite lava (Gardner et al. 2012; Befus et al. 2015b). As a point of reference, we report growth rate (dR/dt) at 600 °C, but emphasize that growth rate is not constant in the model, but instead slows as lava cools.

Temperature of the cooling lava is modeled as a function of time (t) as it changes from T_o to the temperature at which spherulites cease growing (T_F), following

$$T = T_o \exp[-(bt)^{1.5}] \quad (2)$$

where b is a fit parameter. This functional form reproduces the shape of the temperature-time path of numerical conductive cooling models of lava (Manley 1992; Gardner et al. 2012). All magmas of interest were stored at 750 ± 25 °C (Befus and Gardner 2016), and so we set T_o = 750 °C.

In all calculations the diffusivity (D) for each element varies as a function of temperature, following the model equations proposed by Zhang et al. (2010) for rhyolitic melts. In most cases, the equation for D takes the form

$$D = \exp\left[c - \frac{d}{T}\right] \quad (3)$$

where c and d are fit parameters based on experimental data.

Gardner et al. (2012) showed that, for a given growth rate, gradients in the concentrations of incompatible elements are expected to evolve from Type 3 to Type 2 to Type 1 as either cooling rate slows or T_o increases. A similar evolution is expected as growth rate increases under a given thermal regime. Of the elements analyzed, Li is the only one that occurs in Type 1 profiles (Fig. 5). Using the diffusivity model for Li in Zhang et al. (2010), and assuming reasonable estimates for cooling and growth rates (Befus et al. 2015b), the occurrence of Li in Type 1 profiles suggests that all spherulites grew when $T > 350$ °C. If they had continued to grow at much colder temperatures, Li diffusion would become slow enough relative to spherulite growth that it would form Type 2 gradients. Most other elements of interest form Type 3 gradients, with equal concentrations inside and outside of the spherulite. Of those that form Type 3, Sr is expected to diffuse the fastest at relevant conditions, based on the models of Zhang et al. (2010). If $T > 700$ °C, however, Sr diffusion would become fast enough that it would be expected to form Type 2 gradients. The absence of such gradients for Sr concentrations thus argue that spherulites grew at temperatures of 700 °C or colder. We thus assume that most spherulites grew while temperature was between ~350 and ~700 °C.

Support for those relatively cold temperatures for growth of Yellowstone spherulites comes from the observation that they all crosscut flow banding in the samples, instead of deflecting or distorting it. The lack of deflection argues that the Yellowstone spherulites grew while the lava was instead glassy, and hence when temperature was below the glass transition (T_g). If spherulites grew while the lava was still molten, then their growth tends to deflect flow banding (Castro et al. 2008; Watkins et al. 2009; von Aulock et al. 2013). For Yellowstone rhyolite, T_g is estimated at 610–700 °C, using the viscosity model of Giordano et al. (2008) and assuming that $T_g \sim T$ at which viscosity = 10^{12} Pa·s. That range suggests that most spherulites nucleated and grew at temperatures below ~600 °C.

Both the growth history of a spherulite and the thermal conditions during its growth are recorded in the relative enrichment of Type 2 elements, and how far those elements diffuse away from the margin (Watson and Muller 2009; Gardner et al. 2012; Befus et al. 2015b). Here, we define Rb enrichment (ε) as the ratio of its maximum concentration at the margin to its far-field concentration in the matrix, and then convert it to a percentage. The distance away from the spherulite margin that Rb is enriched above the far-field concentration is defined as its propagation distance (P_Δ). We calculate P_Δ as the distance from the margin that the Rb concentration is greater than two standard deviations above that measured in the far-field matrix (Befus et al. 2015b). Befus et al. demonstrated that the ratio (ε/P_Δ) is greater for spherulites that grow faster, at a given cooling rate (Fig. 6a). Conversely, ε/P_Δ decreases for slower cooling rate, for a given growth rate.

The ratio ε/P_Δ has been calculated for every spherulite-glass pair and is plotted vs. the size of the spherulite in Figure 6. Also shown are ε/P_Δ vs. radius for model spherulites, with each curve representing iterative solutions to the numerical moving boundary diffusion modeling using Equations 1–3. Curves in Figure 6 labeled with growth rates were constructed by specifying a growth rate, and solving the equations for a range of possible cooling rates. Curves labeled with cooling rates were each calculated by fixing cooling rate and systematically changing growth rate. The cloud of data formed by the samples covers permissible ranges for parameters in Equations 1 and 2. For temperature, the "permissible" range for b = 3.3 to 32.7, corresponding to cooling rates of 0.0063 to 0.063 °C/h. Regression of the entire set gives a best fit for $b = 9.5^{+14.5}_{-3.0}$, which equals a cooling rate solution of $0.60^{+0.6}_{-0.3}$ °C/day. When b is set to 9.5 and $(dR/dt)_o$ is modified in the growth law equation, the full range of data can be explained by (dR/dt) between 0.2 to 2.0 μm/h, with the entire set best fit by a growth rate of 1.0 ± 0.5 μm/h, again defined as the value at 600 °C, recognizing that the rate decreases exponentially with decreasing T.

Nucleation temperatures of spherulites

We can determine the temperature at which each spherulite nucleated by assuming a given cooling rate and specifying a growth rate. Our modeling of compositional gradients surrounding spherulites indicates that all spherulites grew on average at 1 μm/h (when T = 600 °C), while the lavas cooled at a rate of ~0.6 °C/day. Cooling temperatures and slowing growth with time is supported by the observation that crystal sizes in large spherulites decrease from their interiors to their rims (Fig. 3). In addition, small spherulites, thought to nucleate at colder temperatures than large ones, are fine grained like those in the outer parts of the large spherulites.

Based on the average rates of growth and cooling, the sizes of spherulites in each sample suggest that nucleation temperature ranges between 480 and 600 °C (Figs. 7 and 8). Those temperatures vary, however, if the rates of cooling and growth differ. Spherulites would need to nucleate at hotter temperatures if they grew more slowly under faster cooling. Indeed, given

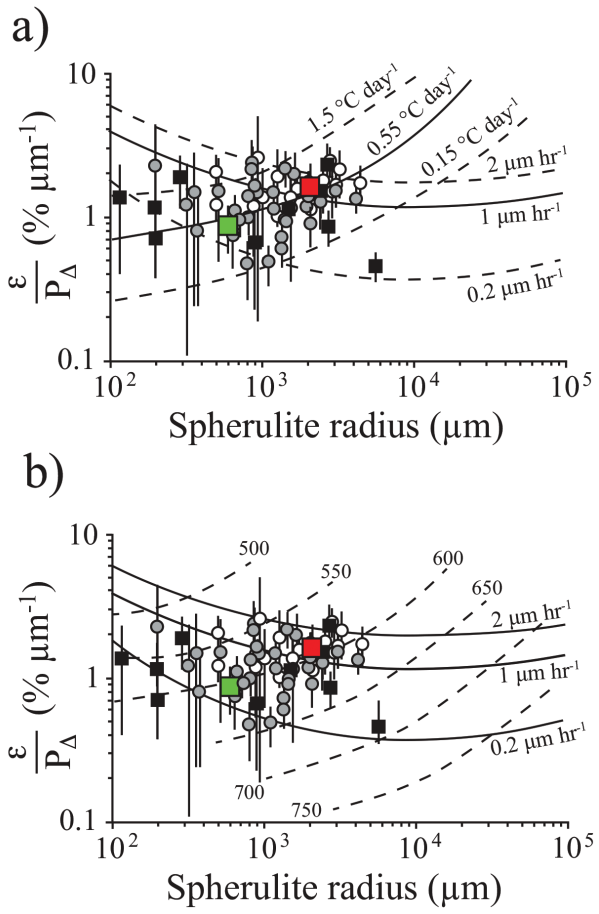

FIGURE 6. The ratio of Rb enrichment (ε) to propagation distance (P_Δ) for 63 spherulite–matrix glass pairs as a function of the diameter of the spherulite measured in 20 samples from the three targeted lava flows (see Fig. 1). Black squares are data from the samples scanned by HRXCT, gray circles are data from other spherulites (Befus, unpublished data), and white circles are data from Befus et al. (2015b). Red square is spherulite Y142 T1 and green square is Y193 T1 (Fig. 5). (**a**) Variations in the ratio expected as a function of cooling rate and growth rate are shown as curves. The best-fit rates for the entire data set are solid curves, whereas dashed curves show the range of permissible rates. (**b**) Variations in the ratio expected given the best-fit cooling rate, for different growth rates (solid curves) and nucleation temperatures (dashed curves).

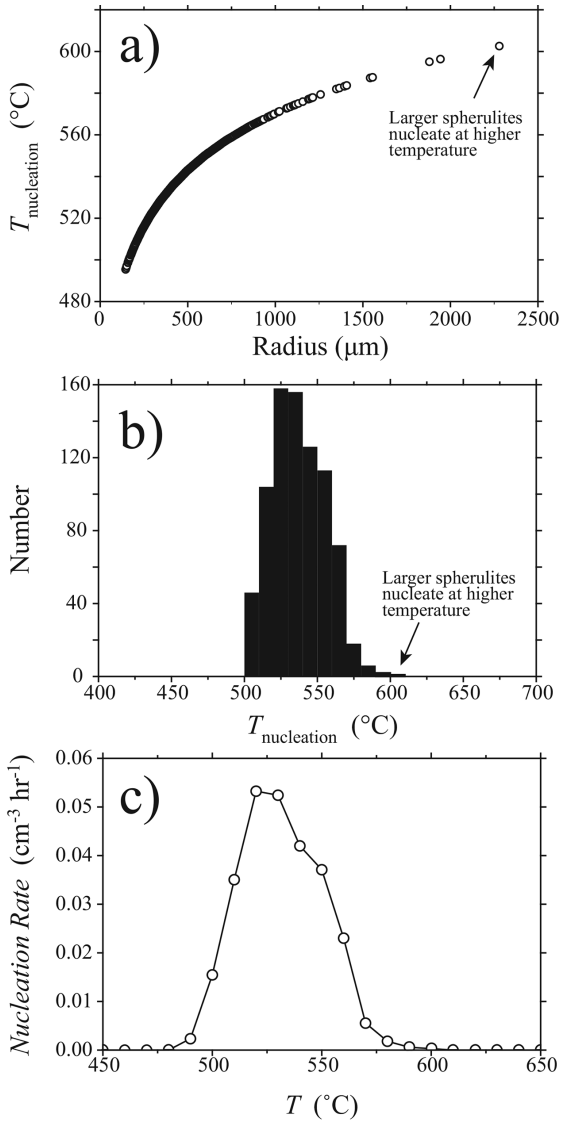

FIGURE 7. Example output for sample Y142, using the best-fit growth rate and cooling rate. (**a**) Nucleation temperature calculated for each spherulite in the sample, once growth rate and cooling rate are specified. (**b**) Histogram of numbers of spherulites nucleated in intervals of 10 °C. (**c**) Volumetric nucleation rate for each bin in **b** calculated with knowledge of the sample size (spherulites + glass) and the amount of time lapsed between each 10 °C interval of cooling.

the spread in rates inferred from the compositional gradients (Figs. 6a and 6b), spherulites would have nucleated at 590–710 °C under the fastest cooling and slowest growth permissible. Conversely, spherulites would nucleate at colder temperatures if they grew faster under slower cooling, and in fact under the slowest permissible cooling and fastest growth, they would have nucleated at 430–500 °C.

Nucleation rates of spherulites

Our modeling suggests that spherulites of similar size nucleate at about the same temperature (Fig. 7a). We thus arbitrarily group spherulites together that nucleated within a temperature window of 10 °C, which defines the number of spherulites nucleated per 10 °C (Fig. 7b). The cooling rate of the sample defines the amount of time that lapsed between each 10 °C interval. As for the volume in which spherulites can nucleate, it shrinks over time as previously nucleated spherulites continue to grow. Because no spherulites were seen to have grown inside other ones, we can assume that the final volume of each spherulite after it stops growing equals the volume in which no later spherulite could have nucleated. This is the same as saying that there is a halo of matrix around a growing spherulite in which no other spherulite can nucleate. The "effective" volume available for nucleation at any given time (temperature) thus equals the total sample volume minus the sum of the final volumes of all

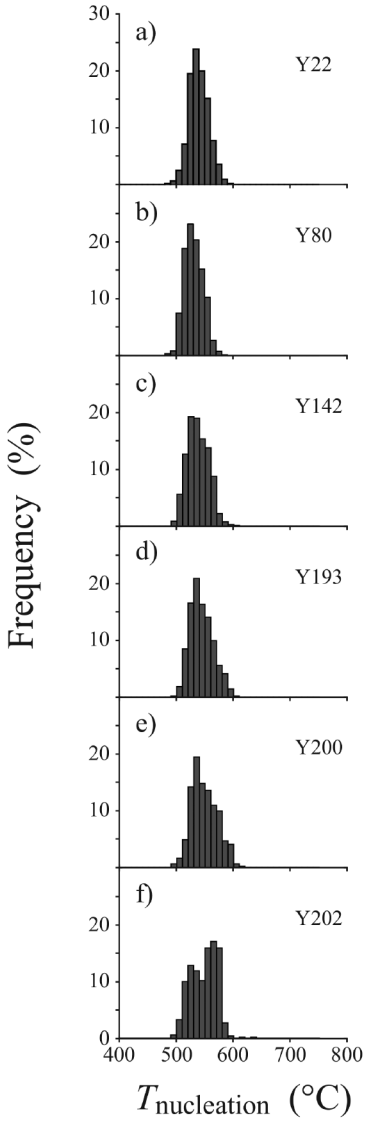

FIGURE 8. Frequency of nucleation temperatures (°C) for spherulites. (**a**) Y22; (**b**) Y80; (**c**) Y142; (**d**) Y193; (**e**) Y200; and (**f**) Y202.

spherulites that had nucleated previously (at higher temperature). The reported nucleation rate for each sample is the number of spherulites nucleated in 10 °C intervals per effective unit volume per unit time (Fig. 7c).

We calculate nucleation rates for the six samples separately to establish the range in rates (Fig. 9). Assuming best-fit rates for growth and cooling (Fig. 6), nucleation, on average, begins at 592 ± 8 °C, and the rate of nucleation accelerates greatly to a peak of 0.072 ± 0.049 cm^{-3} h^{-1} at 533 ± 14 °C. Upon further cooling, nucleation slows until it ceases at 485 ± 6 °C. More generally, nucleation rate depends on assumed rates of cooling and growth. Under the fastest permissible cooling, peak nucleation rates increase to 0.232 (±0.163) to 0.245 (±0.180) cm^{-3} h^{-1}, depending on growth rate. Under conditions of extremely slow cooling, nucleation rate slows to 0.025 (±0.018) to 0.028 (±0021)

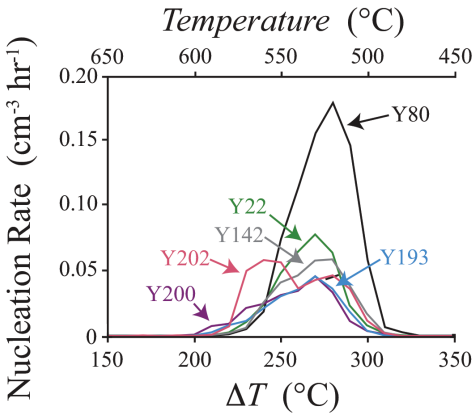

FIGURE 9. Nucleation rates of spherulites for the six Yellowstone rhyolite samples as functions of undercooling ΔT [= $T_L - T_{nucleation}$, with T_L assumed to be 800 °C].

cm^{-3} h^{-1}. The distribution of nucleation rates for most samples is unimodal, and only slightly skewed toward higher temperature. In one case (Y202), however, there is a bimodal distribution of nucleation rates spread out over a wider range of temperatures. The secondary peak at higher temperature is the reflection of the greater number of large spherulites in that sample.

Crystals nucleate in melt/glass at temperatures below the liquidus temperature (T_L), which is defined as the degree of undercooling, ΔT (= $T_L - T$) (e.g., Lofgren 1971). For the sanidine+quartz spherulites in Yellowstone lavas we assume that T_L equals the highest temperature at which both sanidine and quartz crystallize together. Quartz joins sanidine as a crystallizing phase at ~800 °C at 25 MPa in hydrous Yellowstone rhyolite (Befus and Gardner 2016). Extrapolating to 0.1 MPa places the upper limit of their co-precipitation at slightly above 800 °C, because the stability curve for quartz is nearly vertical in pressure-temperature space. We thus assume that T_L for Yellowstone spherulites is 800 °C. Given that assumption, spherulites nucleated under best-fit conditions at $\Delta T \approx 208$ (±6) to 315 (±8)°C (Fig. 9). More generally, $\Delta T \approx$ 100–203 to 277–365 °C, given the permissible ranges in the rates of growth and cooling rate. Regardless of absolute values of ΔT, however, the nucleation interval spans a temperature range of roughly ~88–113 °C.

The peak in spherulite nucleation is inferred by this study to have occurred at $\Delta T = 155$ (±14) to 331 (±16) °C for the ranges in rates of growth and cooling. Under best–fit conditions, $\Delta T =$ 267 (±14) °C. Overall, therefore, nucleation begins when $\Delta T \approx$ 0.65–0.88 × T_L, and peaks when $\Delta T \approx$ 0.59–0.80 × T_L. The peak rate thus occurs at $\Delta T \approx \frac{2}{3} T_L$, which is expected from classical nucleation theory (Lasaga 1998). We note that almost all relatively large spherulites have some phenocryst in their cores, and thus seem to have nucleated heterogeneously.

COMPARISON TO PREVIOUS STUDIES

Recently, Befus (2016) measured oxygen isotopic fractionation between quartz and alkali feldspar ($\Delta^{18}O_{Qtz\text{-}Kfs}$) in Pitchstone Plateau spherulites and found that $\Delta^{18}O_{Qtz\text{-}Kfs}$ is 1.3 ± 0.7‰ in their cores. Such fractionation implies the spherulites

nucleated at 578 ± 160 °C. It was also found that $\Delta^{18}O_{Qtz\text{-}Kfs}$ increases to 2.9 ± 1.1‰ near spherulite rims, which implies that spherulites continued to grow until 301 ± 88 °C, well below T_g. The agreement in nucleation temperatures and the thermal regime for growth between the studies (Fig. 8), which used independent methods, lends strong support to the nucleation rates derived in this study.

In an experimental decompression study of the crystallization of Yellowstone rhyolite, Befus et al. (2015a) found that alkali feldspar microlites nucleated at $\Delta T \geq 60$ °C, but only after 24–120 h at low pressure. Clinopyroxene nucleated under similar conditions as alkali feldspar. In this case, crystallization was driven by loss of dissolved H_2O from the melt, and thus ΔT equates to how much the mineral liquidus temperature is raised above the experimental temperature (Hammer and Rutherford 2002; Befus et al. 2015a). Quartz joined alkali feldspar only when ΔT reached ≥120 °C, and they co-precipitated in coarse crystal aggregates that appear granophyric in texture. They did not form spherical aggregates of closely packed crystals. Our results are consistent with these experimental results, in that dense spherulites appear to require significantly higher ΔT to nucleate and grow. Indeed, Befus et al. (2015a) demonstrated that most microlites in the matrix of Yellowstone lavas grew before lava emplacement, and hence prior to the development of spherulites.

Experimental studies of igneous textures, especially in rhyolitic melts, often only report nucleation densities, because of the uncertainties in conditions for nucleation. Swanson (1977) reported number densities of feldspars and quartz nuclei in hydrous silicic melts and found that they increased dramatically as ΔT increased, from <10 cm^{-3} at ΔT < 100 °C to >$10^{7–8}$ cm^{-3} at ΔT > 200 °C. Fenn (1977) reported nucleating 10^3–$10^{3.8}$ feldspar spherulites per cm^{-3} in hydrous feldspathic melt at ΔT ≥ 110 °C. In comparison, spherulites in Yellowstone lavas occur in number densities of 74–314 cm^{-3}, and they nucleated at ΔT = 100–365 °C. The significantly lower nucleation density at greater ΔT for natural rhyolite can most likely be attributed to the impact of dissolved H_2O on nucleation rate. Both Fenn (1977) and Swanson (1977) used melts with ~2–12 wt% H_2O, which is significantly more than that in matrix glasses of Yellowstone lavas (~0.1–0.2 wt%). Greater H_2O contents are known to significantly accelerate diffusion (Zhang et al. 2010) and lower viscosity (Giordano et al. 2008), both of which enhance nucleation (e.g., Swanson and Fenn 1986). Greater H_2O contents also lowers T_g (Deubener et al. 2003), which would allow spherulites to nucleate while rhyolite is still molten, also enhancing nucleation.

Spherulites grown experimentally generally change in texture from coarse and open at low ΔT, to "bow tie" shaped at moderate ΔT, to round and dense with small crystals at high ΔT (Lofgren 1971; Swanson 1977; Swanson et al. 1989). The latter type tend to grow at ΔT > 250–300 °C (Lofgren 1971; Swanson 1977). Yellowstone spherulites are generally spherical and closely packed with small crystals (relative to the size of the spherulite) and lack obvious bow-tie structures (Fig. 1). It is noteworthy that dense, fine-grained Yellowstone spherulites are inferred to have grown at ΔT of ~250 °C, similar to experiments, despite differences between experimental and natural samples.

Concluding remarks

Spherulites measured in Yellowstone obsidian lavas range in size from 0.006 to 460 mm^3, with median volumes of 0.19–0.99 mm^3. Geochemical gradients preserved around spherulites indicate that most grew while the lavas cooled at 0.30 to 1.20 °C/day, at rates that decreased exponentially with temperature and time, but were 0.2 to 2.0 μm/h at 600 °C. Between 74 and 314 cm^{-3} spherulites nucleated during cooling and mostly formed unimodal, symmetrical distribution of sizes. Growth occurred over a range of temperatures, consistent with the variations in crystal sizes, and mostly at or below the glass transition temperature of the matrix, consistent with the lack of deformation of the matrix by the spherulites. Depending on rates of cooling and growth, nucleation temperatures fall between ~430 to ~710 °C, but the actual range in temperature is much narrower for a specific set of conditions. Peak nucleation rates of 0.072 ± 0.049 cm^{-3} h^{-1} are found at ΔT = 267 (±14) °C, using best-fit approximations for the rates of cooling and growth. The nucleation rates derived in this study provide estimates that are appropriate for nearly anhydrous rhyolite, which have not been measured experimentally.

Acknowledgments

We thank Nathan Miller for his help with the LA-ICP-MS analyses and Rich Ketcham and Jesse Maisano for their help with X-ray computed tomography data collection and analysis. This research was made possible by grants from the National Science Foundation to J.E.G. (EAR-1049829) and J.M.W. (EAR-1249404), and a National Park Service research permit (YELL-05678). Funding for HRXCT scanning was provided in part by NSF grant EAR-1258878 to R. Ketcham, T. Rowe, and W. Carlson. J.E.G. wishes to thank the Institute for Advanced Studies, Durham University, for their hospitality during preparation of this manuscript.

References cited

Albarede, F., and Bottinga, Y. (1972) Kinetic disequilibrium in trace element partitioning between phenocrysts and host lava. Geochimica et Cosmochimica Acta, 36, 141–156.

Befus, K.S. (2016) Crystallization kinetics of rhyolitic melts using oxygen isotope ratios. Geophysical Research Letters, 43, doi:10.1002/2015GL067288.

Befus, K.S., and Gardner, J.E. (2016) Magma storage and evolution of the most recent effusive and explosive eruptions from Yellowstone caldera. Contributions to Mineralogy and Petrology, doi:10.1007/s0041-016-1244-x.

Befus, K.S., Manga, M., Gardner, J.E., and Williams, M. (2015a) Ascent and emplacement dynamics of obsidian lavas inferred form microlite textures. Bulletin of Volcanology, 77, doi:10.1007/s00445-015-0971-6.

Befus, K.S., Watkins, J., Gardner. J.E., Richard, D., Befus, K.M., Miller, N.R., and Dingwell, D.B. (2015b) Spherulites as in-situ recorders of thermal history in lava flows. Geology, 43, 647–650.

Bowen, N.L. (1919) Crystallization differentiation in igneous magmas. Journal of Geology, 27, 393–430.

——— (1947) Magmas. Bulletin of the Geological Society of America, 58, 263–280.

Cashman, K.V., and Marsh, B.D. (1988) Crystal size distribution (CSD) in rocks and the kinetics and dynamics of crystallization; 2, Makaopulu lava lake. Contributions to Mineralogy and Petrology, 99, 292–305.

Castro, J.M., Beck, P., and Tuffen, H. (2008) Timescales of spherulite crystallization in obsidian inferred from water concentration profiles. American Mineralogist, 93, 1816–1822.

Christiansen, R.L. (2001) The Quaternary and Pliocene Yellowstone Plateau Volcanic Field of Wyoming, Idaho, and Montana. U.S. Geological Survey Professional Paper 729-G, 145 p.

Christiansen, R.L., Lowenstern, J.B., Smith, R.B., Heasler, H., Morgan, L.A., Nathenson, M., Mastin, L.G., Muffler, L.J.P., and Robinson, J.E. (2007) Preliminary assessment of volcanic and hydrothermal hazards in Yellowstone National Park and vicinity. U.S. Geological Survey Open-file Report 2007-1071, 94 p.

Deubener, J., Müller, R., Behrens, H., and Heide, G. (2003) Water and the glass transition temperature of silicate melts. Journal of Non-Crystalline Solids, 330, 268–273.

Fenn, P.M. (1977) The nucleation and growth of alkali feldspars from hydrous melts. Canadian Mineralogist, 15, 135–161.

Gardner, J.E., Befus, K.S., Watkins, J., Hesse, M., and Miller, N. (2012) Compositional gradients surrounding spherulites in obsidian and their relationship to

spherulite growth and lava cooling. Bulletin of Volcanology, 74, 1865–1879.
Giordano, D., Russell, J.K., and Dingwell, D.B. (2008) Viscosity of magmatic liquids: A model. Earth and Planetary Science Letters, 271, 123–134.
Hammer, J.E., and Rutherford, M.J. (2002) An experimental study of the kinetics of decompression-induced crystallization in silicic melt. Journal of Geophysical Research, 107, doi:10.1029/2001JB000281.
Hanna, R.D., Ketcham, R.A., Zolensky, M., and Behr, W.M. (2015) Impact-induced brittle deformation, porosity loss, and aqueous alteration in the Mutchison CM chondrite. Geochimica et Cosmochimica Acta, 171, 256–282.
Higgins, M.D. (1999) Origin of megacrysts in granitoids by textural coarsening: A crystal size distribution (CSD) study of microcline in the Cathedral Peak granodiorite, Sierra Nevada, California. Geological Society of London Special Publications, 168, 207–219.
Johannes, W. (1979) Ternary feldspars: Kinetics and possible equilibria at 800°C. Contributions to Mineralogy and Petrology, 68, 221–230.
Ketcham, R.A. (2005) Computational methods for quantitative analysis of three-dimensional features in geological specimens. Geosphere, 1, 32–41.
Lasaga, A.C. (1998) Kinetic Theory in the Earth Sciences, 811 p. Princeton University Press, New Jersey.
Lofgren, G. (1971) Experimentally produced devitrification textures in natural rhyolitic glass. Bulletin of the Geological Society of America, 82, 111–124.
Lofgren, G.E. (1974) An experimental study of plagioclase crystal morphology: isothermal crystallization. American Journal of Science, 274.
Manley, C.R. (1992) Extended cooling and viscous flow of large, hot rhyolite lavas: Implications of numerical modeling results. Journal of Volcanology and Geothermal Research, 53, 27–46.
Marsh, B. (1988) Crystal size distribution (CSD) in rocks and the kinetics and dynamics of crystallization. Contributions to Mineralogy and Petrology, 99, 277–291.
——— (1998) On the interpretation of crystal size distributions in magmatic systems. Journal of Petrology, 39, 553–599.
——— (2007) Crystallization of silicate magmas deciphered using crystal size distributions. Journal of the American Ceramics Society, 90, 746–757.
McKenzie, D. (1984) The generation and compaction of molten rock. Journal of Petrology, 25, 713–765.
Morgan, D.J., Jerram, D.A., Chertkoff, D.G., Davidson, J.P., Pearson, D.G., Kronz, A., and Nowell, G.M. (2007) Combining CSD and isotopic microanalysis: magma supply and mixing processes at Stromboli Volcano, Aeolian Islands, Italy. Earth and Planetary Science Letters, 260, 419–431.
Schairer, J.F., and Bowen, N.L. (1956) The system Na_2O–Al_2O_3–SiO_2. American Journal of Science, 254, 129–195.
Smith, V.G., Tiller, W.A., and Rutter, J.W. (1955) A mathematical analysis of solute redistribution during solidification. Canadian Journal of Physics, 33, 723–745.
Swanson, S.E. (1977) Relation of nucleation and crystal-growth rate to the development of granitic textures. American Mineralogist, 62, 966–978.
Swanson, S.E., and Fenn, P.M. (1986) Quartz crystallization in igneous rocks. American Mineralogist, 71, 331–342.
Swanson, S.E., Naney, M.T., Westrich, H.R., and Eichelberger, J.C. (1989) Crystallization history of Obsidian Dome, Inyo Domes, California. Bulletin of Volcanology, 51, 161–176.
Turnbull, D. (1948) Transient nucleation. Transactions of the American Institute of Mineral Engineering, 175, 174–783.
von Aulock, F.W., Nichols, A.R.L., Kennedy, B.M., and Oze, C. (2013) Timescales of texture development in a cooling lava dome. Geochimica et Cosmochimica Acta, 114, 72–80.
Watkins, J., Manga, M., Huber, C., and Martin, M. (2009) Diffusion-controlled spherulite growth in obsidian inferred from H_2O concentration profiles. Contributions to Mineralogy and Petrology, 157, 163–172.
Watson, E.B., and Muller, T. (2009) Non-equilibrium isotopic and elemental fractionation during diffusion-controlled crystal growth under static and dynamic conditions. Chemical Geology, 267, 111–124.
Winkler, H.G.F. (1947) Kristallogrosse und Abkuhlung. Heidelberger Beitr. Mineralogie und Petrology, 1, 86–104.
Zhang, Y., Ni, H., and Chen, Y. (2010) Diffusion data in silicate melts. Reviews in Mineralogy and Geochemistry, 72, 311–408.

Manuscript received November 12, 2015
Manuscript accepted May 23, 2016
Manuscript handled by Julia Hammer